Internal Flow Physics of a Fluidic Oscillator in the Transition Regime

Mehmet N. Tomac and James W. Gregory

Abstract. An experimental investigation of the underlying flow physics of a dual jet interaction fluidic oscillator has been conducted in the transition regime for a Reynolds number of 1680. The transition regime is defined as a narrow range of flow rates between two other operating modes of the fluidic oscillator. Particle image velocimetry (PIV) was used with refractive index matching sodium iodide solution to minimize reflections from the actuator geometry and obtain detailed internal velocity fields. PIV results showed that the interaction of the two internal jets and the resultant vortices are responsible for the oscillation mechanism in the transition regime. Two side vortices sustain their existence throughout the oscillation period by altering their size, shape and strength, and a dome vortex is created twice each oscillation period (once from each jet). The dome vortex plays a key role in the kinetic energy transfer mechanism inside the oscillator by means of jet bifurcations. The primary oscillation mechanism in the transition regime is that each internal jet's connection with the exiting jet is cut completely by the dome vortex in every period. This is in contrast to the low flow rate oscillation mechanism in which the oscillations are created by continuous collisions of the jets. Furthermore, the internal jets were observed to energize the side vortex on the opposite side of the chamber – a phenomenon which was not observed in the low flow rate regime.

Mehmet N. Tomac
Assistant Professor, Abdullah Gul University, Department of Mechanical Engineering, 38039, Kayseri, Turkey
email: mehmet.tomac@agu.edu.tr

James W. Gregory
Associate Professor, The Ohio State University, Department of Mechanical and Aerospace Engineering, 201 W. 19th Ave., Columbus, OH, USA
email: gregory.234@osu.edu

AFCC 2014, Berlin 2014.

1 Introduction

Fluidic oscillators create an unsteady oscillating jet with a frequency that depends primarily on the internal fluid dynamics of the device. They are attracting increased interest in the scientific and industrial flow control communities due to their superior advantages as flow control actuators: they have no moving parts, yet offer high control authority and a wide range of operating frequencies. Fluidic oscillators have recently been used as sweeping jets in flow control applications, but they can also be considered for periodic flow control applications due to their frequency content. While many flow control methods and actuators are under continued investigation at laboratory scales, fluidic oscillators are being used for flow control on full-scale flight vehicle models. NASA and Boeing recently tested a full-scale 757 vertical tail equipped with fluidic oscillators as sweeping jet actuators to maintain attached flow over the rudder across a wide range of flow conditions, with preliminary studies reported in the literature [1].

Characterization of the internal and external fluid dynamics of fluidic oscillators has become important since different flow control applications and flow conditions require a comprehensive understanding of the oscillation mechanisms for thoughtful implementation. Wall attachment fluidic oscillators operate based on the Coanda effect and have been intensively studied since fluidics era of the 1960s (e.g., Warren [2], Spyropoulos [3], Booth [4], Lush [5], Gaylord and Carter [6]). However, this work studies a relatively new type of fluidic oscillator that is based on internal jet collisions and interactions. The collision of opposed jets has been known to yield self-sustained oscillations (Nomoto *et al.* [7], Denschikov *et al.* [8-9], Rolon *et al.* [10], Pawlowski *et al.* [11]) if the certain parameters such as the distance between nozzles and the characteristic jet velocity are selected properly. One of the early fluidic oscillators based on internal jet interactions is the so-called “feedback-free” fluidic oscillator developed by Raghu [12]. This oscillator creates self-sustained oscillations based on the collision of two inclined jets in a dome-shaped mixing chamber. The geometrical outline of this fluidic oscillator can be seen in Fig. 1.

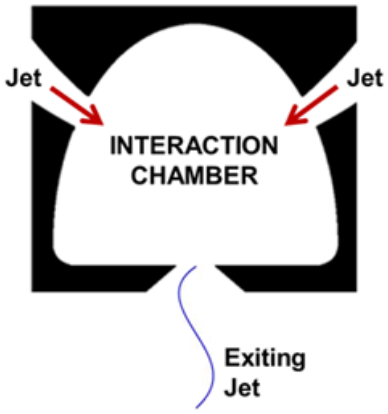

Fig. 1. Feedback-free fluidic oscillator design of Raghu [12].

Gregory *et al.* [13] investigated the internal jet interactions of the feedback-free fluidic oscillator by using pressure-sensitive paint (PSP) and concluded that an unsteady shear layer that is driven by two counter-rotating side vortices governs the oscillation process. In another study, Gregory *et al.* [14] used a micro-scale version of the feedback-free fluidic oscillator to determine the oscillator's external flow characteristics. They reported that the variation of frequency with flow rate is linear, but with a discontinuity in slope at a particular flow rate that was indicative of a change in oscillation modes. In their combined experimental and numerical study, Bidadi *et al.* [15] discussed how the unstable arrangement of the jet interaction creates vortices which eventually dictate the oscillatory behavior. In a preliminary study, Tomac and Gregory [16] used PIV to measure the dual jet interactions in the interaction chamber of a feedback-free fluidic oscillator. They determined the existence of three distinct flow regimes and suggested that there were different oscillation mechanisms depending on the flow rate (Reynolds number). The low flow rate and transition flow rate regimes were observed for very low Re, while the high flow rate regime constituted the normal operating range for that particular scale of fluidic oscillator. The low flow rate behavior was discussed in detail by Tomac and Gregory [17]. They concluded that the two jets collide with each other continuously and neither of the jets is completely cut by the dome vortex which governs the bifurcation and the kinetic energy competition between the two jets.

The transition regime is defined as a narrow range of flow rates between the other two regimes, representing a distinct operating mode from the other two. It is a very interesting operating condition for the fluidic oscillator: further study will help explain why the character of the oscillations changes from the low flow rate to high flow rate regimes. The present study focuses on the details of the jet interactions and oscillation mechanism of the feedback free fluidic oscillators in the transition regime by using refractive index matched particle image velocimetry (PIV) technique. This investigation aims to understand the detailed flow physics of dual jet interactions, jet cut off, kinetic energy transfer mechanisms, vortex-shear layer and vortex-wall interactions, and the overall oscillation mechanism of the feedback-free fluidic oscillator in the transition regime.

2 Experiments

The internal flow field of the feedback-free fluidic oscillator was extracted with the help of refractive index-matched PIV technique together with a custom microphone-tube sensor configuration and a quarter period based PIV phase-averaging method. The details of this experimental setup are described as follows.

2.1 Fluidic Oscillator Model

The fluidic oscillator model used for this investigation was 12.5 *mm* in width, 15 *mm* in length, and 1.5 *mm* in depth. The nozzle width of both internal jets was 1.70 *mm*, and the exit nozzle width was 2 *mm*. The models were fabricated from clear acrylic by laser cutting three parts. These parts were stacked to form the oscillator assembly and secured with acrylic glue. These parts and an assembled fluidic oscillator are shown in Fig. 2. Primary concerns for the fabrication of the oscillator were optical access, geometrical precision, and prevention of any leaks.

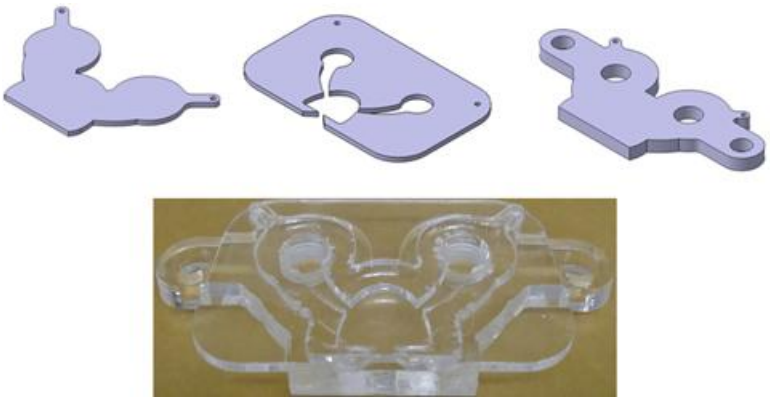

Fig. 2. Isometric view of the three parts (top), and unified fluidic oscillator model (bottom).

2.2 Refractive Index-Matched PIV Technique

PIV was selected to measure the phase-averaged internal flow field resulting from the jet interactions. However, reflections of laser light energy from acrylic-air or acrylic-water interfaces due to differences in refractive index will significantly diminish the quality of the experimental data. To prevent these reflections, a refractive index matched fluid of sodium iodide (NaI) solution was used. The prepared solution consisted of 60% NaI by weight with a density of 1730 kg/m^3 and volume of 5 *L*. Hollow glass spheres were used for seeding, and density differences between the seed and fluid were found to produce negligible buoyancy-induced velocity errors. A schematic of the experimental setup is shown in Fig. 3: a 200 *mJ* double-pulsed Nd:YAG 532 *nm* laser (New Wave Solo XT 200) with sheet-forming optics (spherical and cylindrical lens), a programmable timing unit (LaVison External PTU V. 9.0), and a CCD camera (PCO 1600) with a macro lens (Sigma 105 *mm*, 1:2.8D) were used. The time separation between two laser illuminations was 300 μs and LaVision's Davis software was used for data acquisition and post-processing, in conjunction with LabView 8.6 and MATLAB R2011b.

The flow rate through the oscillator was measured with a flow meter (Omega Engineering FLR1011ST) that was specifically calibrated for the refractive index matching fluid. The synchronization signal for phase averaging was obtained through a microphone-tube sensor configuration

that operates based on a condenser microphone. Fluctuations in the flow rate complicated the phase-averaging process, precluding any *in situ* phase locking efforts. To solve this problem, a quarter-period based PIV phase averaging method was used (the details of which are discussed by Tomac and Gregory [17]).

Six-hundred images were acquired for the flow rate presented in this paper and the period of the oscillations was divided into 40 phases. The maximum number of images in each phase bin was 18 and minimum number of images was 11. Re number was calculated based on the exit width, average velocity at the exit of the oscillator and the kinematic viscosity of the NaI solution at 28.8 °C.

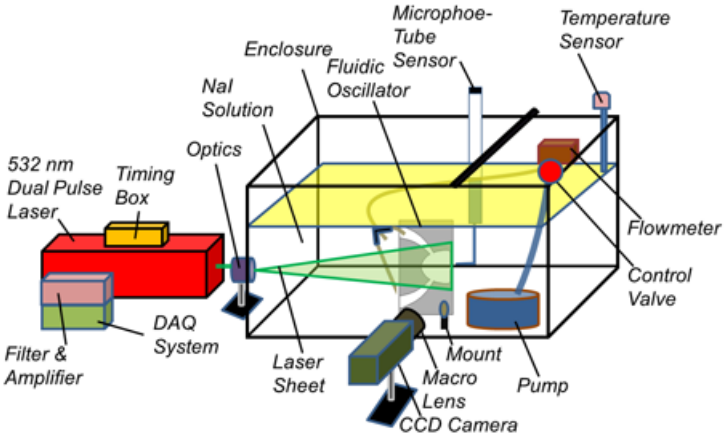

Fig. 3. Schematic of the experimental setup.

3 Results

Tomac and Gregory [16] reported three distinct operating regimes across a range of flow rates from 2.8 mL/s to 15 mL/s as shown in Fig. 4. The transition regime, spanning a narrow range of flow rates from 3.5 to 4.0 mL/s, yielded a plateau region in the flow rate-frequency plot at about 26.5 Hz. The results discussed in this section correspond to a flow rate of 3.5 mL/s (Re = 1680) as indicated by the arrow in Fig. 4. Tomac and Gregory [17] investigated the internal flow field in the low flow rate regime; the current study reveals the differences that distinguish the transition regime from the low flow rate regime even though the predominant oscillation mechanism is similar.

The discussion presented here illuminates the unknown flow physics of dual jet interactions and bifurcations, jet deflection, the role of the side and dome vortices in the oscillation mechanism, and the interaction of the walls with the jets and the vortices in the transition regime.

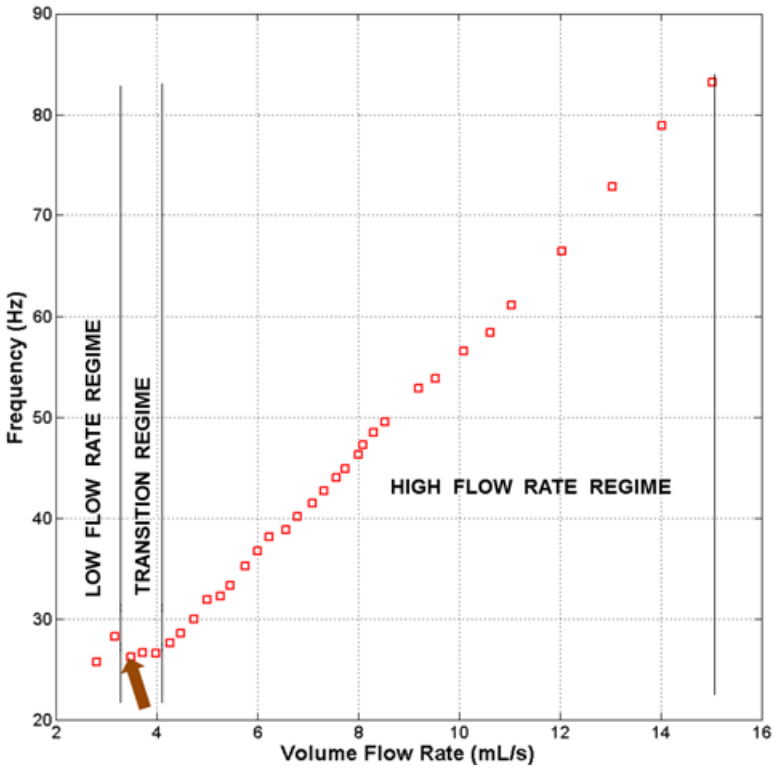

Fig. 4. Frequency characteristics of the fluidic oscillator.

For the purposes of identifying key features in the flow, Fig. 5 shows flow streamlines superimposed onto vorticity contours at one phase within the oscillation period. The two jets create four shear layers in total, two created by the upper jet (3-4) and two created by the lower jet (1-2). The upper jet right shear layer (4) feeds the upper side vortex (7) and the upper jet left shear layer (3) feeds the upper dome vortex (6). Likewise, the lower jet right shear layer (2) feeds the lower side vortex (9) and the lower jet left shear layer (1) feeds the lower dome vortex which does not exist for this phase, but it forms in the other half period of the oscillations. The dome vortices

form and vanish depending on the phase; however, the side vortices persist with changing size, shape and strength. The lower jet of the oscillator is bifurcated, as indicated by the saddle point at (5). The left branch of the bifurcated lower jet coalesces with the upper jet through the dome region (10). Eventually, due to the interaction of all these flow structures an unsteady oscillating exiting jet (8) is created at the exit of the fluidic oscillator.

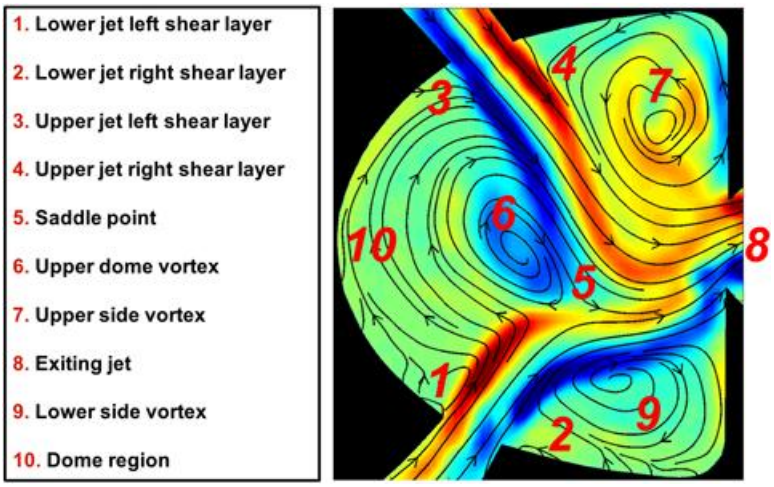

Fig. 5. Nomenclature for internal flow structures and regions.

Fig. 6 shows the streamlines superimposed on the velocity (left) and vorticity (right) contours for 0˚ phase angle. For this phase angle, the main difference from the low flow rate regime [17] can be easily observed. Unlike the low flow rate regime, the lower jet's connection with the exiting jet is completely cut. Instead, it is bifurcated into two branches, neither of which is directly connected with the exiting jet at this instant. The left branch of the lower jet coalesces with the upper jet by transferring some of its kinetic energy to the upper jet. The right branch of the lower jet is forced toward the lower side vortex region and is trapped in this region. The velocity of the lower jet is high enough such that the upper jet is substantially deflected. This deflection of the upper jet causes its potential core to directly energize the lower side vortex. (This was not the case for the low flow rate regime, where both jets collided along the oscillator's centerline and mutually fed the jet exit). At this phase position the potential core of the upper jet is mov-

ing toward the exiting jet to connect with it. The lower side vortex pushes the lower jet toward the dome region, while a lower dome vortex is forming and growing stronger as it constricts the left branch of the lower jet. Furthermore, as the lower side vortex grows stronger, it increases the vorticity of negative sign above the wall next to the exit orifice. At this phase, the upper side vortex is not energized by the upper jet right shear layer and the vorticity present is a remnant from earlier phases.

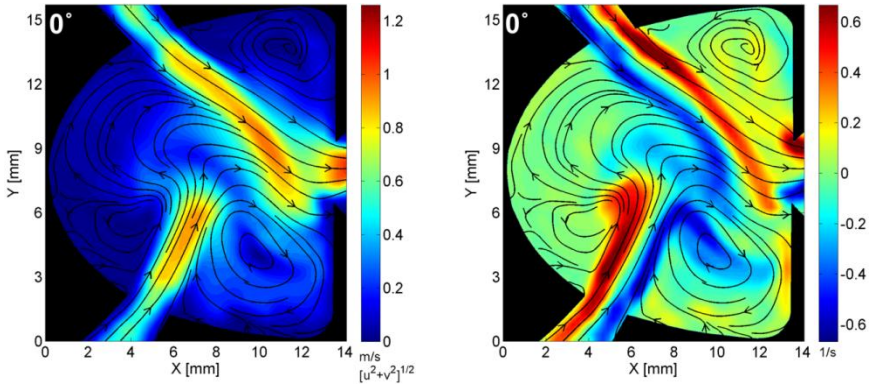

Fig. 6. Streamlines superimposed on velocity (left) and vorticity (right) contours at 0˚ phase angle in the transition regime.

Fig. 7 presents the results for a phase angle of 45˚. As shown, the lower dome vortex has moved toward the upper jet. As it grows, it pushes the lower jet toward the exiting jet and toward the lower side vortex, while constricting the left branch of the lower jet which is coalescing with the upper jet. Although the upper jet is about to cease energizing the lower side vortex since the upper jet core is entirely connected to the exiting jet, the lower jet right shear layer continues to feed the lower side vortex. Furthermore, as the strong lower dome vortex is pushing the lower jet toward the exiting jet and the lower side vortex, the vorticity in the side wall boundary layer is significantly increased from the previous phase shown in Fig. 6.

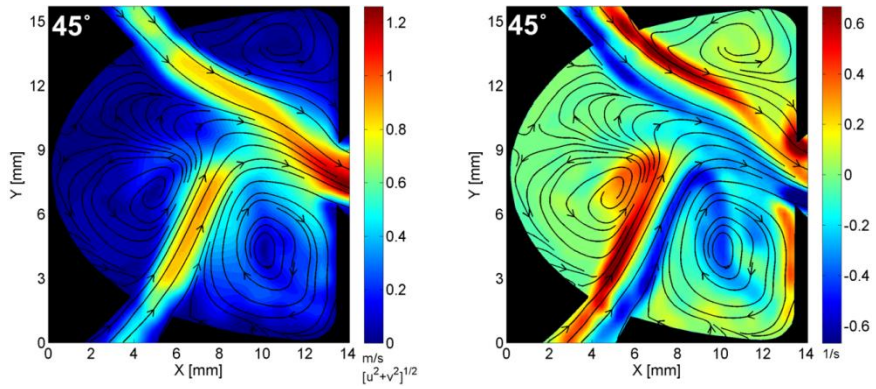

Fig. 7. Streamlines superimposed on velocity (left) and vorticity (right) contours at 45˚ phase angle in the transition regime.

At a phase angle of 90˚ shown, in Fig. 8, the lower dome vortex has reached the upper jet and started bifurcating the upper jet. Due to this bifurcation, the upper jet's left branch flows through the dome region, coalesces with the lower jet, and transfers some of its kinetic energy to the lower jet. The left branch of the upper jet also weakens as the lower dome vortex bifurcates increasing portions of the upper jet. At the same time a small upper dome vortex fed by the upper jet left shear layer starts to form.

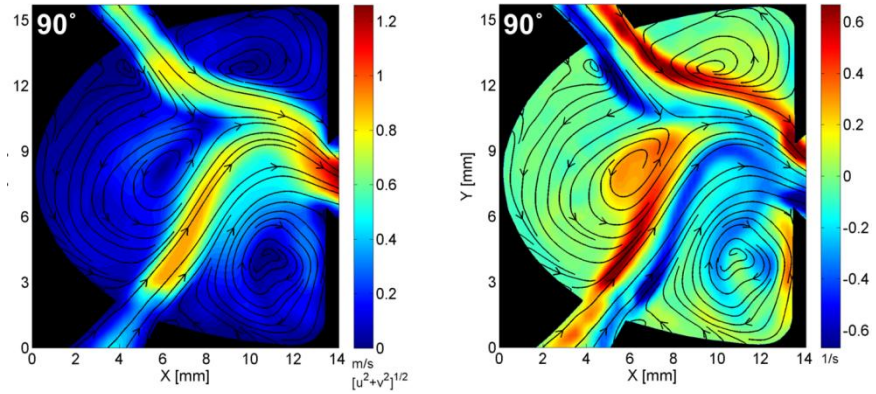

Fig. 8. Streamlines superimposed on velocity (left) and vorticity (right) contours at 90˚ phase angle in the transition regime.

Fig. 9 shows the final phase inside the interaction chamber of the fluidic oscillator in the transition regime before the upper jet is completely cut by the lower dome vortex. At this instant, the upper jet left branch is coalescing with the lower jet and its right branch is still connected with the exiting jet. The size and the strength of the lower side vortex are decreased significantly and it is not being energized by the lower jet right shear layer any longer. Furthermore, the upper jet right shear layer is being pushed toward the upper side vortex region; however, it is not energizing the upper side vortex since the jet is still connected with the exiting jet. Nevertheless, as the upper jet right shear layer gets closer to the wall near the exit orifice, the vorticity in the wall boundary layer is increased slightly.

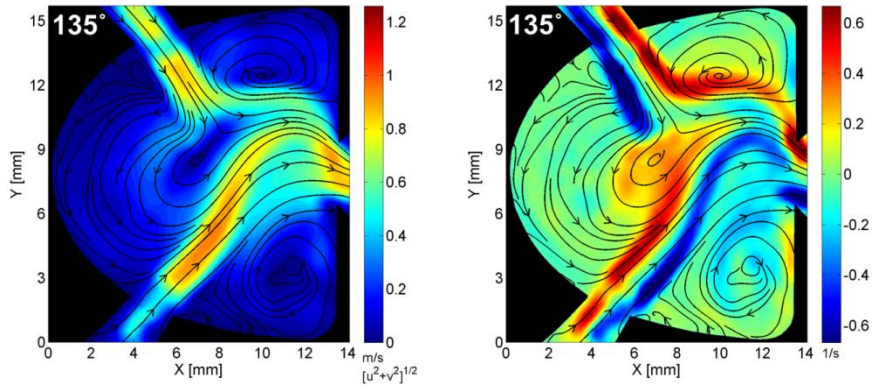

Fig. 9. Streamlines superimposed on velocity (left) and vorticity (right) contours at 135˚ phase angle in the transition regime.

For the phase angle of 180˚ shown in Fig. 10, the results are simply the mirrored images of the results presented at the beginning of the oscillation period. This time the upper jet is cut, while the lower jet energizes the upper side vortex before its core connects with the exiting jet and the upper dome vortex is formed by the upper jet left shear layer. Note that, for this instant the lower jet left shear layer energizes the upper side vortex and the lower jet right shear layer energizes the lower side vortex. Furthermore, in the transition regime side and dome vortices were observed to be stronger than the vortices created in the low flow rate regime and consequently the strength of the vorticity created over the walls has also increased.

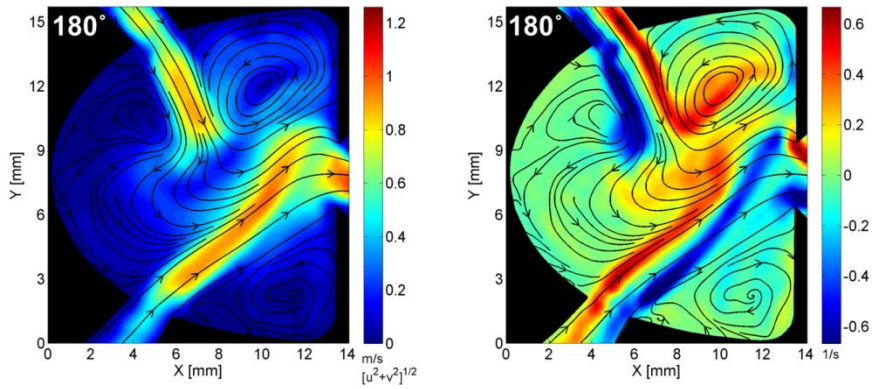

Fig. 10. Streamlines superimposed on velocity (left) and vorticity (right) contours at 180˚ phase angle in the transition regime.

The latter half of the oscillation cycle displays a similar mechanism to that just described. As seen in Fig. 11, the upper dome vortex grows and pushes the upper jet toward the exit while constricting the left branch of the upper jet. The lower jet potential core is connected to the exiting jet at this instant. Fig. 12 shows the contours of velocity and vorticity before the dome vortex-saddle point collision. In Fig. 13, which displays results for a phase angle of 351˚, the saddle point collision has already occurred and has completely cut the connection of the lower jet's potential core with the exiting jet.

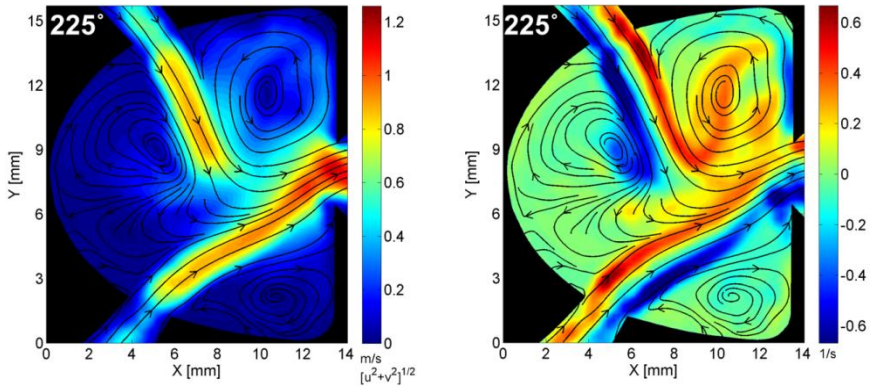

Fig. 11. Streamlines superimposed on velocity (left) and vorticity (right) contours at 225˚ phase angle in the transition regime.

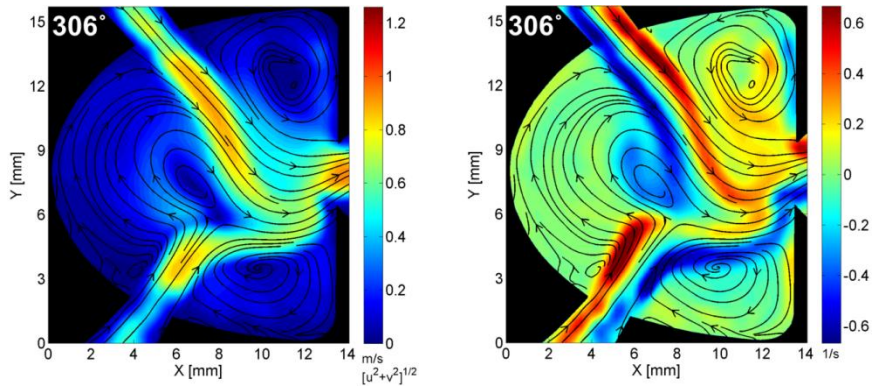

Fig. 12. Streamlines superimposed on velocity (left) and vorticity (right) contours at 306° phase angle in the transition regime.

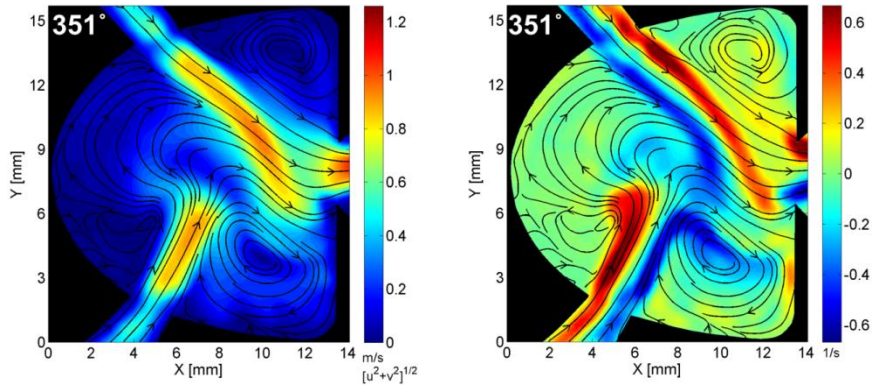

Fig. 13. Streamlines superimposed on velocity (left) and vorticity (right) contours at 351° phase angle in the transition regime.

4 Conclusion

Details of internal flow physics and oscillation mechanism of a feedback-free type fluidic oscillator in the transition regime at Re of 1680 were extracted by using a refractive index-matched PIV technique along with a custom made microphone-tube sensor configuration and a quarter period based PIV phase-averaging method. Refractive index matched PIV results indicated the creation of two side and two dome vortices by the shear layers of the

jets. Dome vortices were observed to appear and vanish throughout the period and are mainly responsible for the jet bifurcation and kinetic energy transfer. Persistent side vortices trigger the creation of the dome vortices as they change their size, shape and strength continuously. As the jet is bifurcated by a dome vortex, its connection with the exiting jet weakens. This connecting portion is deflected by the opposing jet, causing the exiting jet's flow direction to alter continuously until the jet connection is cut completely with the exiting jet. Also in the transition regime, the side vortices (lower side and upper side) are also periodically energized by the opposite jet in addition to the shear layer that is already energizing them — unlike the low flow rate regime in which most of the kinetic energy transferred to the side vortices was acquired from the corresponding shear layer of the nearest jet.

Oscillatory behavior in the transition regime is a consequence of many interesting flow physics features such as jet collisions, interactions, bifurcations, cutting and bending, vortex-shear layer and vortex-wall interactions. In contrast to the oscillation mechanism in the low flow rate regime, each jet's connection with the exiting jet is completely cut by the dome vortex in every period and the kinetic energy of the bifurcated jet is transferred to the jet that creates the dome vortex. This kinetic energy transfer mechanism overrides the fact that the flow rates of the jets are equal and there is no reason for a jet to be the dominant supplier of the exiting jet.

References

1. Seele, R., Graff, E., Lin, J., and Wygnanski, I., "Performance Enhancement of a Vertical Tail Model with Sweeping Jet Actuators," AIAA 2013-0411, *Proceedings of the 51st AIAA Aerospace Sciences Meeting*, Grapevine, TX, 2013.

2. Warren, R. W., and Peperone, S. J., "Fluid Amplifications. 1. Basic Principles," Report. No. TR-1039, Diamond Ordnance Fuze Labs, Aug. 15, 1962.

3. Spyropoulos, C. E., "Sonic Oscillator," *Proceedings of the Fluid Amplification Symposium*, Vol. 3, Harry Diamond Laboratories, Washington, D.C., 1964, pp. 27-51.

4. Booth, W. A., "Performance Evaluation of a High-Pressure-Recovery Bistable Fluid Amplifier," Fluid Jet Control Devices, *Proceedings of the Symposium on Fluid Jet Control Devices at the Winter Annual Meeting of the ASME*, New York, NY on Nov 28, 1962, pp. 83-90.

5. Lush, P.A., "A Theoretical and Experimental Investigation of the Switching Mechanism in a Wall Attachment Fluid Amplifier," *Proceedings of IFAC Symposium on Fluidics*, London, Nov. 1968.

6. Gaylord, W., and Carter, V., *Fluerics 27: Flueric Temperature-Sensing Oscillator Design*, Harry Diamond Laboratories, Washington, D.C., Apr. 1969, HDL TR-1428, accession number AD0689444.

7. Nomoto, A., Yamamoto, K., and Ohshio, Y., "Axial impingement of two bounded jets," *Proceedings of the 2nd International JSME Symposium on Fluid Machinery and Fluidics*, Tokyo, Japan, 1972, pp. 71-80.

8. Denshchikov, V.A., Kondrat'ev, V.N., and Romashov, A.N., "Interaction between two opposed jets," *Fluid Dynamics*, Vol. 13(6), 1978. pp. 924-926. doi: 101007/BF01050971.

9. Denshchikov, V.A., Kondrat'ev, V.N., Romashov, A.N., and Chubarov, V.M., "Auto-oscillations of planar colliding jets," *Fluid Dynamics*, Vol. 18(3), 1983. pp. 460-462. doi: 101007/BF01090570.

10. Rolon, J.C., Veynante, D., and Martin, J.P., "Counter jet stagnation flows," *Exp Fluids*, Vol. 11, 1991, pp. 313–324.

11. Pawlowski, R.P., Salinger, A.G., Shadid, J.N., and Mountziaris, T.J., "Bifurcation and stability analysis of laminar isothermal counterflowing jets," *J Fluid Mech*, Vol. 551, 2006, pp. 117-139.

12. Raghu, S., "Feedback-Free Fluidic Oscillator and Method," U.S. Patent 6,253,782, Issued July 3, 2001.

13. Gregory, J.W., Sullivan, J.P., and Raghu, S., "Visualization of Jet Mixing in a Fluidic Oscillator," *J Visual*, Vol. 8(2), 2005, pp. 169-176.

14. Gregory, J.W., Sullivan, J.P., Raman, G., and Raghu, S., "Characterization of the Microfluidic Oscillator," *AIAA Journal*, Vol. 45(3), 2007, pp. 568-576.

15. Bidadi, S., Heister, S.D., and Matsutomi, Y., "Computational and Experimental Study of Jet Interaction Fluidic Injectors," *Atomization Spray*, Vol. 21(2), 2011, pp.127-138.

16. Tomac, M.N., and Gregory, J.W., "Frequency studies and scaling effects of jet interaction in a feedback-free fluidic oscillator," AIAA 2012-1248, *Proceedings of the 50th AIAA Aerospace Sciences Meeting*, Nashville, TN, 2012.

17. Tomac, M.N. and Gregory, J.W., "Internal Jet Interaction in a Fluidic Oscillator at Low Flow Rate," *Exp Fluids*, 55:1730, 2014. Also see Tomac, M.N. and Gregory, J.W., "Jet Interactions in a Feedback-Free Fluidic Oscillator at Low Flow Rate," AIAA 2013-2478, *Proceedings of the 43rd AIAA Fluid Dynamics Conference*, San Diego, CA, 2013.